inorganics

MDPI

Article

Low-Cost Carbon Nanoparticles for Removing Hazardous Organic Pollutants from Water: Complete Remediation Study and Multi-Use Investigation

Babiker Y. Abdulkhair [1,2,*] and Mohamed R. Elamin [1]

[1] Chemistry Department, Faculty of Science, Imam Mohammad Ibn Saud Islamic University (IMSIU), P.O. Box 90950, Riyadh 11623, Saudi Arabia
[2] Chemistry Department, Faculty of Science, Sudan University of Science and Technology (SUST), Khartoum 13311, Sudan
* Correspondence: byabdulkhair@imamu.edu.sa or babiker35.by@gmail.com

Abstract: Continuous waste discharge into natural water resources in many countries is a severe global issue, and seeking an effective solution is a researcher's concern. Herein, toilet paper waste was a low-cost precursor for preparing carbon nanoparticles (TPCNPs). The characterization of TPCNPs revealed a 30 nm to 50 nm particle size, a 264 m^2 g^{-1} surface area, and a cubical graphite lattice XRD pattern. The TPCNPs were tested for removing malachite green (MG), indigo carmine (IC), rhodamine B (RB), and methylene blue (MB) dyes from water. The solution parameters were examined for the sorption process, and a pH of 5.0 suited the MB removal, while a pH of 6.0 was suitable for MG, IC, and RB. The effect of concentration investigation showed an adsorption capacity of 110.9, 64.8, 73.5, and 98 mg g^{-1} for MG, IC, RB, and MB, respectively. The sorption of the four dyes fitted the Langmuir isotherm model; it was exothermic and spontaneous. The water remediation was tested using groundwater and seawater samples (GW and SW) spiked with pollutants. It is worth mentioning that one treatment sufficed for the remediation of GW and SW contaminated by 5 mg L^{-1} concentration, while a double treatment was required for 10 mg L^{-1} pollution in both samples.

Keywords: carbon nanoparticles; toilet paper waste; malachite green; indigo carmine; rhodamine B; methylene blue

Citation: Abdulkhair, B.Y.; Elamin, M.R. Low-Cost Carbon Nanoparticles for Removing Hazardous Organic Pollutants from Water: Complete Remediation Study and Multi-Use Investigation. *Inorganics* **2022**, *10*, 136. https://doi.org/10.3390/inorganics10090136

Academic Editor: Carlos Martínez-Boubeta

Received: 13 August 2022
Accepted: 2 September 2022
Published: 7 September 2022

1. Introduction

The continuous waste discharge into natural water resources causes severe drinking and irrigation water problems worldwide [1,2]. This spread of pollutants in the water environment results from the rapid industrialization trend [3,4]. Organic dyes with an azo-group, aromatic rings, or sulphonate groups are toxic and carcinogenic [5]. Many techniques have been employed to remove such pollutants from water, including flocculation, chemical oxidation, ion exchange, and membranes [6–9]. The detection of organic dyes in the tap water of some first-world countries makes evident the failure of conventional treatments to keep such contaminants from drinking water [10–13]. Conversely, the adsorption process is a successful method for removing such pollutants [10–14]. Mainly, the adsorption binding forces may include hydrogen bonding, π-π bonding, induced dipole interaction, and van der Waals forces [15]. The sorbate's polarity and the adsorbent's pore size, surface area, and functionality can affect the removal efficiency. The traditional use of carbonaceous materials (CRMs) as a color or odor remover from solutions draws attention because of its outstanding adsorbing capacities [16]. In addition, the low-cost, safety, ease of use, and high surface area make the carbonaceous allotropes a potential water treatment substrate [17]. Carbonaceous allotropes may include activated carbon, nanotubes, nanofibers, graphene, and nanoparticles. Unlike metal-oxide nanomaterials, the precursors for fabricating CRMs are of high diversity. In addition, the surface of CRMs can be easily modified through

implanting functional groups, which increases their adsorbing properties significantly [18]. CRMs can be prepared from many virgin precursors, but because of the influential cost factor, it is better to fabricate CRMs from waste. Therefore, lemonwood, orange peels, potato shells, and various agricultural wastes were studied. Many researchers target CRMs as cheap sorbents for removing water contamination [19–25]. This study aimed to prepare carbon nanoparticles from waste toilet paper (TPW) as a low-cost precursor and to use the produced CRMs would be ground via a ball-milling process as an available downsizing method to produce carbon nanoparticles (TPCNPs). The prepared sorbent will be employed to eliminate malachite green (MG), indigo carmine (IC), rhodamine B (RB), and methylene blue (MB) from seawater and groundwater samples. Moreover, the number of cycles required for completely remediating contaminated water will be studied.

2. Results and Discussion

2.1. Characterization of TPCNPs

The SEM results in Figure 1a,b revealed clustered particles attributed to the milling process. The separate particles appeared within a size range of 40 to 76 nm. In addition, the elemental composition of the TPCNPs was determined using EDX. As monitored in Figure 1c,d, the TPCNPs comprised 84.4% carbon and 15.6% oxygen. The high oxygen content indicated the successful implanting of oxygen-functional groups.

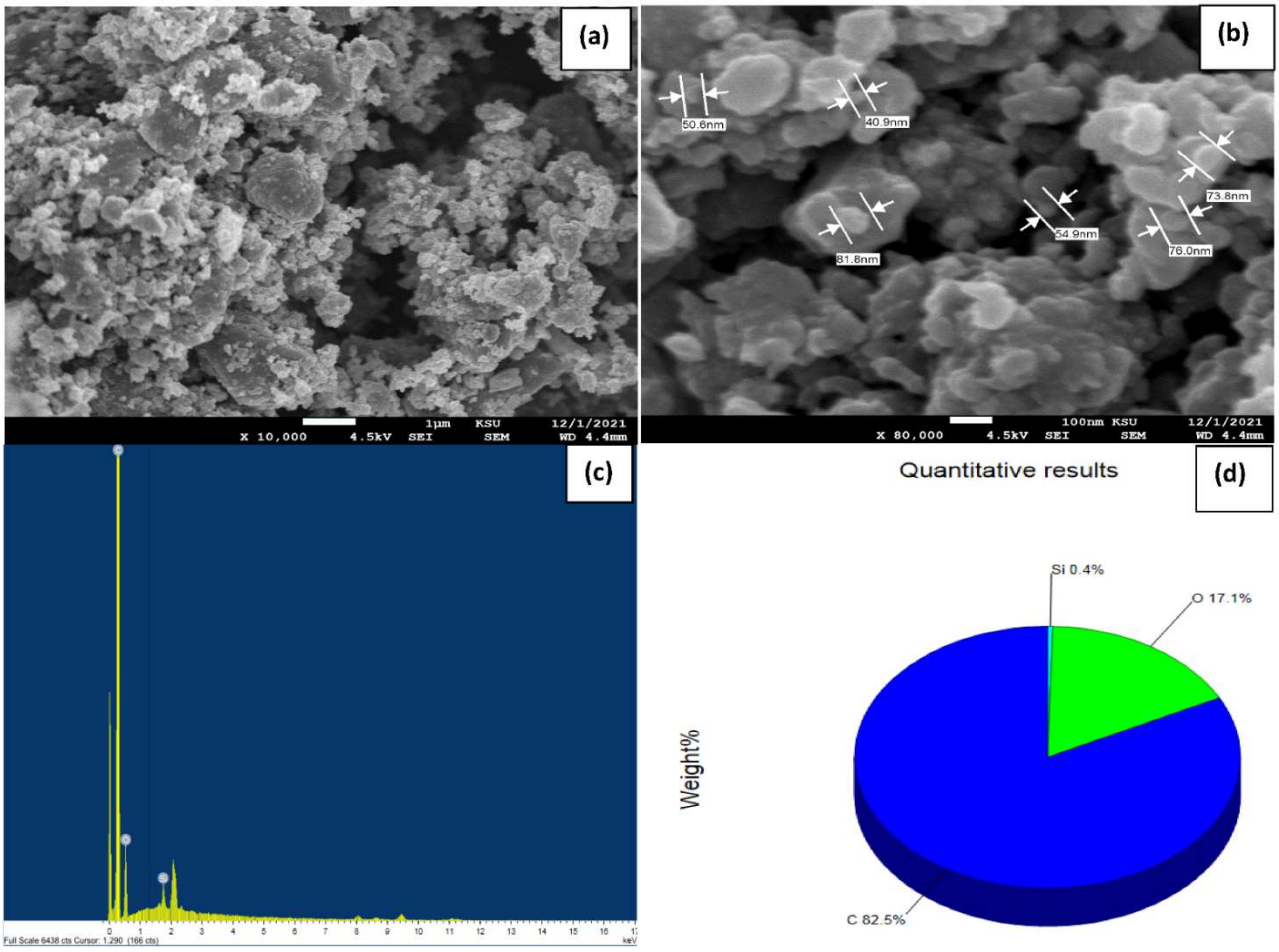

Figure 1. (**a**,**b**) SEM results for the fabricated TPCNPs; (**c**,**d**) EDX spectrum and the elemental composition for the prepared TPCNPs.

Figure 2a shows the XRD results for the produced TPCNPs. The diffraction peaks at 2θ° of 23.71 and 44.48 can be assigned to (002) and (100) of the cubical lattice graphite phase (JCPDS no. 04-0850) [26–28]. Moreover, the baseline elevation at 2θ° of 10 can be

attributed to uncrystallized carbon and/or agglomerated by the milling process [29]. The average crystal size of TPCNPs was calculated with Scherrer's equation (Equation (1), and the lattice parameters (*a* and *c*) were estimated via Equations (2) and (3), while the lattice imperfection (ε) was calculated via Equation (4) [29,30].

$$D = \frac{0.9\lambda}{\beta \cos\theta} \quad (1)$$

$$a = \frac{\lambda}{\sqrt{3}\, sin\theta} \quad (2)$$

$$c = \frac{\lambda}{sin\theta} \quad (3)$$

$$\varepsilon = \frac{\beta}{4\, cos\theta} \quad (4)$$

where θ, λ, and β represent the Bragg's angle, $Cu\text{-}K_{\alpha}$ line (1.5406 Å), and the peak width at half-maximum [31]. The lattice parameters were calculated using the two principal peaks, and their findings are illustrated in Table 1.

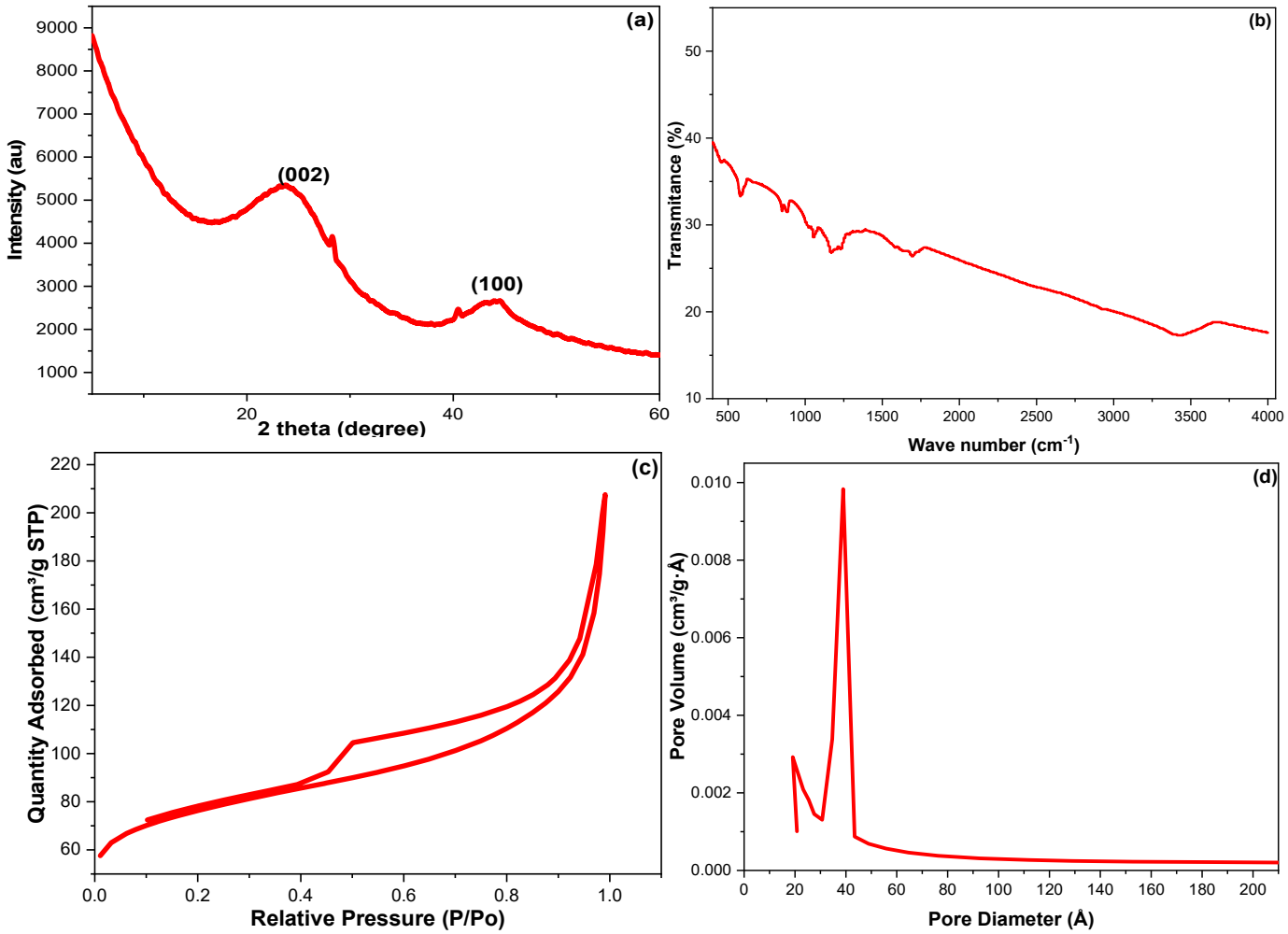

Figure 2. (**a**) the XRD pattern, (**b**) the FTIR bond-vibration bands, (**c**) the nitrogen adsorption–desorption isotherm, and (**d**) pore size distribution for the fabricated TPCNPs.

Table 1. The lattice parameters for the prepared TPCNPs as calculated from the XRD spectrum.

Parameters	23.7083 (2θ°)	44.4823 (2θ°)	Avge
D (nm)	0.414	2.079	1.246
a (nm)	0.183	0.337	0.260
c (nm)	7.500	4.070	5.785
ε (Arbutary)	0.377	0.356	0.367

The FT-IR analysis was employed to explore the functional groups on the TPCNPs, and the obtained vibration bands are illustrated in Figure 2b. The peaks around 1300 cm^{-1} and 1720 cm^{-1} are most likely C-O and C=O stretching vibrations of carboxylic groups; the OH band between 3000 cm^{-1} and 3600 cm^{-1} supports this conclusion. The C=C stretching vibration of the graphitic structure was indicated via the 1640 cm^{-1} band; the symmetric and asymmetric C-H stretching vibrations were assigned to the peaks near 2850 cm^{-1} and 2930 cm^{-1}, respectively [32,33]. These results demonstrated that TPW was successfully carbonized at 900 °C, and the nitric acid treatment succeeded in implanting oxygen-functional groups, which aligns with the EDX results.

Figure 2c,d show the nitrogen adsorption–desorption isotherm and the pore volume distribution for the TPCNPs. The hysteresis loop type (III) possessed by TPCNPs indicated a mesoporous material with various pore volumes (PV) [34]. The Brunauer–Emmett–Teller (BET) method was utilized for determining the surface area (SA), while the Barrett–Joyner–Halenda (BJH) method was used to estimate the pore diameter (PD) and PV of the TPCNPs. The obtained SA, PD, and PV values were 264.52 m^2 g^{-1}, 37.12 Å, and 0.26 cm^3 g^{-1}, respectively. These findings were comparable to some carbonaceous materials in the literature [35–37].

2.2. Adsorption of Organic Dyes by TPCNPs

The adsorption of IC, RB, MG, and MB from aqueous solutions by the prepared TPCNPs was studied. The time influence on the adsorption of the four dyes was monitored in Figure 3a. All sorbent/sorbate systems took 120 min to attain equilibrium, except for MB, which required only 90 min. The evaluation of pH impact (Figure 3b) showed that pH 5.0 was suitable for removing MB, while pH 6.0 was appropriate for removing MG, IC, and RB. In addition, these results are somewhat expected since an alkaline medium may convert these dyes to their salt forms and thus prefer to stay in water over being adsorped, which is in line with the literature results [38–40].

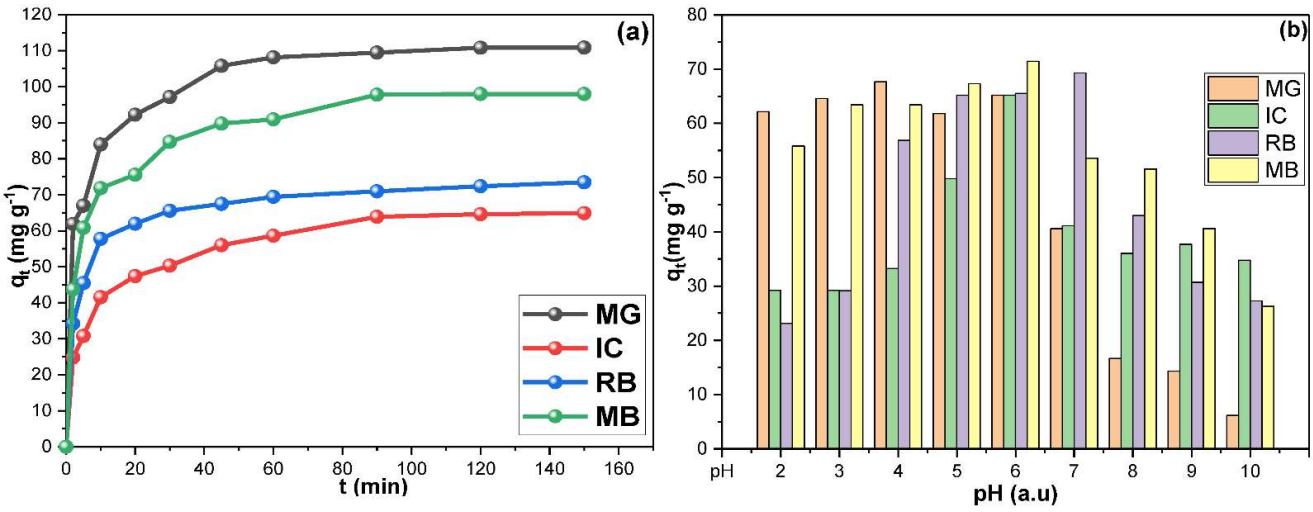

Figure 3. (**a**) the contact time study and (**b**) the impact of pH on the adsorption of MG, IC, RB, and MB on the synthesized TPCNPs.

Furthermore, the four dyes' sorption was studied by utilizing four different concentrations at three different temperatures. Figure 4 shows that the q_t increased proportionally with the fed concentration and inversely with the solution temperature. At 20 °C, the q_t values of MG, IC, RB, and MB reached 116.2, 109.5, 144.6, and 147.8 mg g^{-1}, which are competitive results compared to recent literature findings [41–48]. The high adsorption capacity of the 100 mg L^{-1} solutions inferred the usability of this sorbent for industrial waste treatment where such pollutants were released at high concentrations. Figure 4 also indicated that the sorbent: solution ratio of 4:5 was suitable even for high pollutant concentrations. On the other hand, the semi-complete remediation of water contaminated by 10 mg L^{-1} nominated TPCNPs for efficient treatment of polluted water resources where low concentrations were expected. Moreover, the adsorption of MG, IC, RB, and MB on the TPCNPs decreased inversely as the temperature rose (Figure 4). These findings implied an exothermic nature of the adsorption of the four dyes.

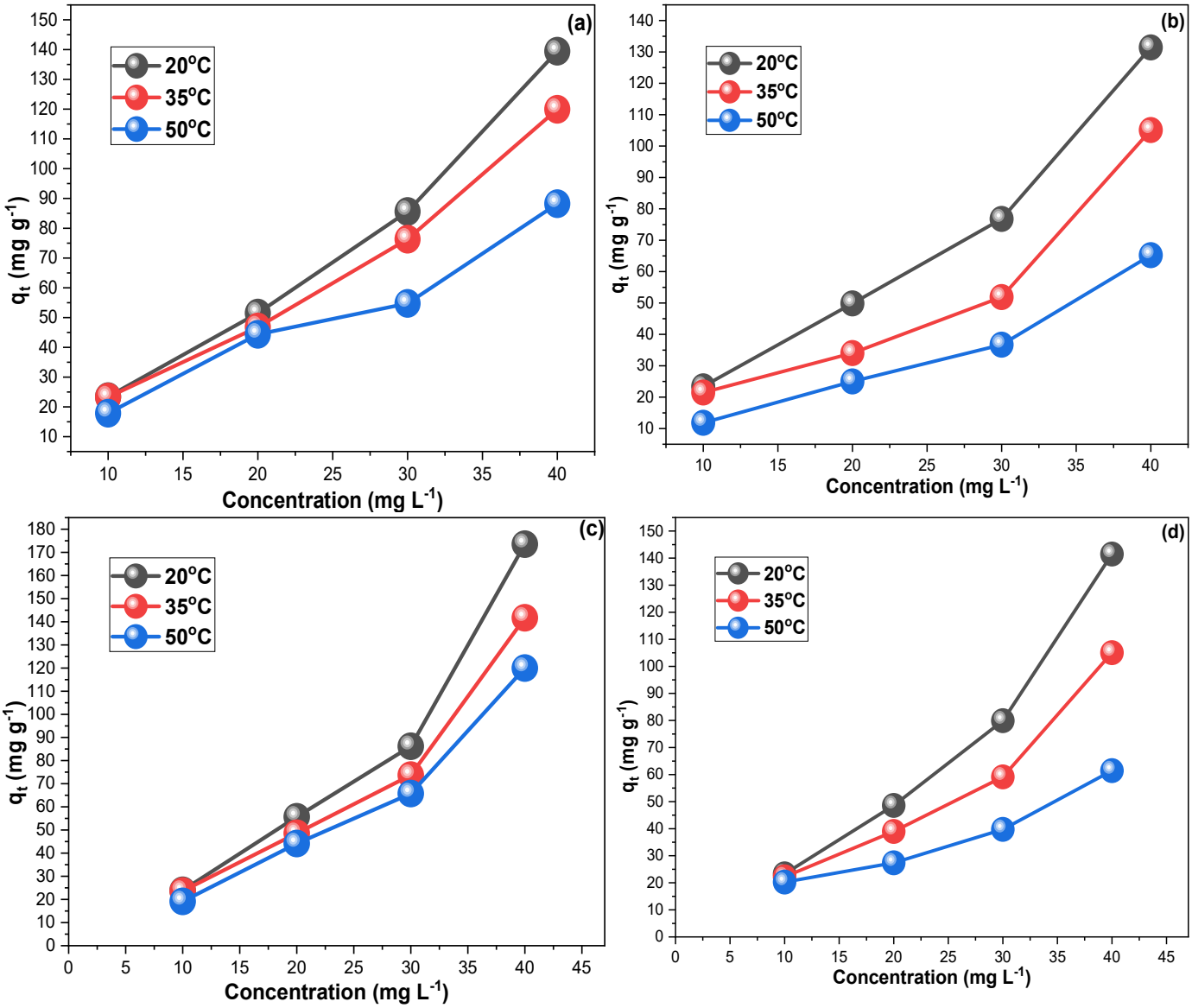

Figure 4. The influence of solution concentration on the removal by the TPCNPs at 20 °C, 35 °C, 50 °C for (**a**) MG, (**b**) IC, (**c**) RB, and (**d**) MB.

2.3. Adsorption Kinetics

The pseudo-first-order (PSFO) and pseudo-second-order (PSSO) kinetic models (Equations (5) and (6)) were used to investigate the adsorption rates of MG, IC, RB, and MB on TPCNPs. In addition, to better understand the adsorption, the sorption control step was inspected via the intra-particle and liquid film diffusion models (IPDM and LFDM) expressed in Equations (7) and (8).

$$\ln(q_e - q_t) = ln(q_e) - kt \quad (5)$$

$$\frac{1}{q_t} = \frac{1}{k_2 q_e^2 t} + \frac{1}{q_e} \quad (6)$$

$$q_t = K_{ip} * t^{\frac{1}{2}} + C_i \quad (7)$$

$$ln(1 - F) = -K_{LF} * t \quad (8)$$

k_1 (min^{-1}), k_2 (g mg^{-1} min^{-1}), K_{ip} (mg g^{-1} $min^{-0.5}$), and K_{LF} (min^{-1}) were the PSFO, PSSO, IPDM, and LFDM constants, respectively; q_e and q_t (mg g^{-1}) were the adsorbed amount of dye on a gram of TPCNPs at equilibrium and time t. C_i (mg g^{-1}) is a parameter related to the boundary layer thickness. Figure 5 illustrates the regression plots of the adsorption rate order and the rate control mechanism. The extracted slope and intercept values were employed in calculating k_1, k_2, K_{ip}, and K_{LF} [49]. The results gathered in Table 2 indicated that MG and IC adsorption on the TPCNPs fitted the PSFO model with higher R^2 values. Based on these findings, the sorbent–sorbate interaction occurred via diffusion through the TPCNP boundaries, which suggests physisorption. In contrast, RB and MB followed the PSSO model, indicating an association of chemisorption mechanisms in removing RB and MB dyes [50–53]. Furthermore, the rate control mechanism investigations for the four dyes' adsorption revealed that LFDM was the slowest step in controlling the adsorption of the four dyes (Table 2).

Table 2. The kinetics parameters for MG, IC, RB, and MB adsorption on the prepared TPCNPs by stirring 120 mL of 50mg L^{-1} pollutant solution with 50 mg TPCNPs.

Adsorption Kinetic								
Adsorption Rate Order								
	PSFO				PSSO			
Dye	MG	IC	RB	MB	MG	IC	RB	MB
q_e exp. (mg g^{-1})	110.852	64.883	73.452	97.974	110.852	64.883	73.452	97.974
q_e cal. (mg g^{-1})	45.480	41.885	25.887	65.048	102.249	56.180	69.979	91.241
R^2 (Arbutary)	0.971	0.973	0.905	0.891	0.840	0.920	0.984	0.975
Rate constant	0.042	0.038	0.029	0.055	0.007	0.006	0.007	0.005
Adsorption Mechanism								
Pollutant ↓	Intraparticle Diffusion Model (IPDM)				Liquid Film Diffusion Model (LFDM)			
	K_{IP} (mg g^{-1} $min^{0.5}$)	C (mg g^{-1})	R^2		K_{LF} (min^{-1})	R^2		
MG	5.218	62.980	0.854		−0.042	0.972		
IC	4.124	24.983	0.919		−0.038	0.967		
RB	3.461	40.689	0.770		−0.029	0.905		
MB	5.162	49.595	0.862		−0.055	0.892		

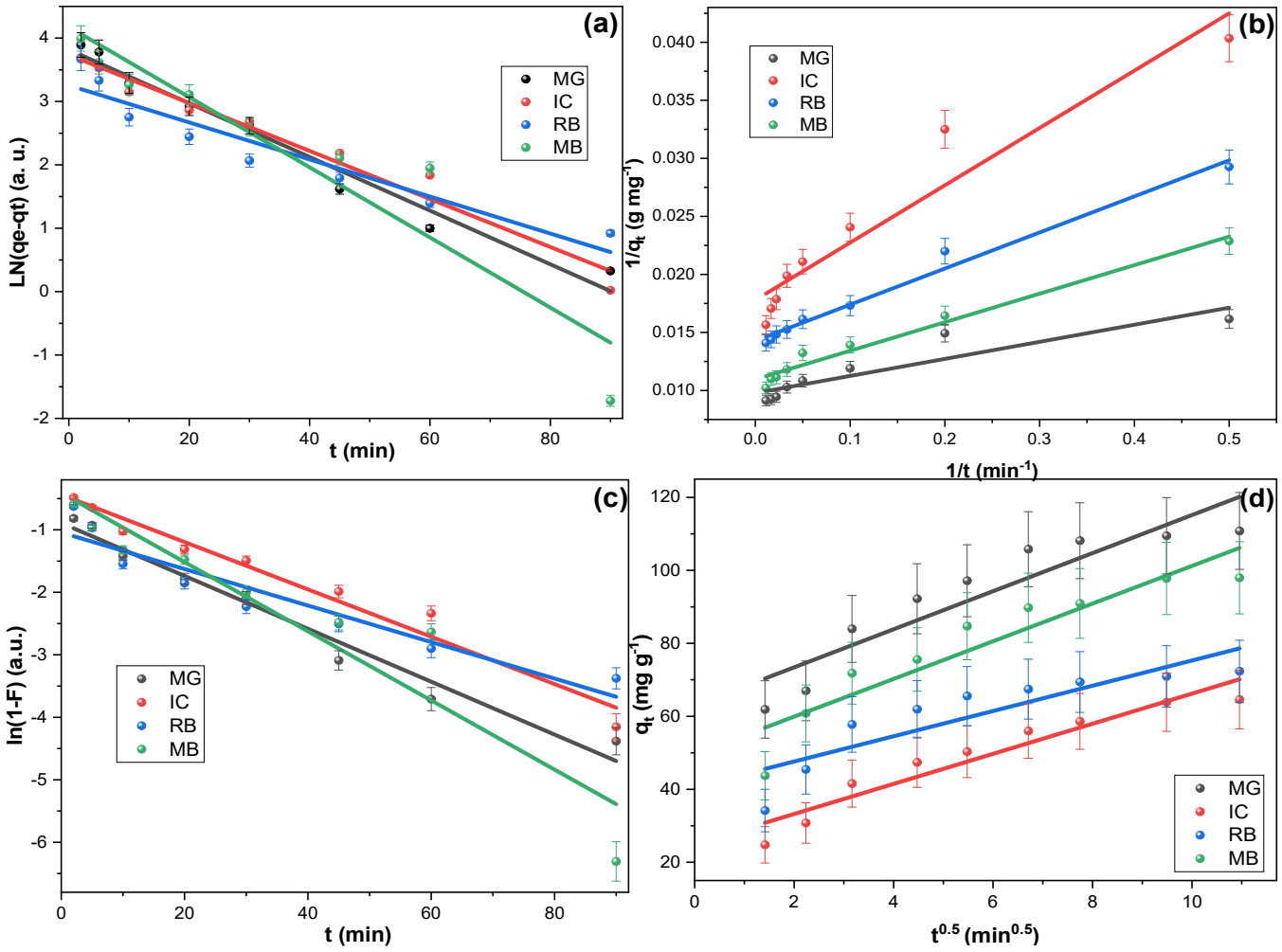

Figure 5. (**a**) PSFO, (**b**) PSSO (**c**) LFDM (**d**) IPDM investigations for the adsorption of MG, IC, RB, and MB dyes on the TPCNPs at 25 °C.

2.4. Adsorption Isotherms

Numerous models in the literature were used to describe the adsorption isotherm; among these, the Langmuir (LIM, Equation (9)) and Freundlich models (FIM, Equation (10)) were the most used ones. Herein, both models were employed to investigate the removal of MG, IC, RB, and MB from TPCNPs.

$$\frac{1}{q_e} = \frac{1}{K_l\, q_m} \cdot \frac{1}{C_e} + \frac{1}{K_l} \tag{9}$$

$$\ln q_e = \ln K_f + \frac{1}{n}\, \ln C_e \tag{10}$$

K_L (L mg^{-1}) and K_F (L mg$^{-1)}$ represent LIM and LFM constants; C_e (mg L^{-1}) is the unadsorbed concentration at equilibrium, q_m is the calculated maximum adsorption capacity, and $1/n$ is the Freundlich adsorption intensity [54]. Figures 6 and 7 illustrated LIM and FIM fittings for the adsorption of the four dyes on the TPCNPs, and their findings were gathered in Table 3. The sorption of the four dyes on TPCNPs appeared to have a better fit to FIM. Additionally, the obtained $1/n$ values for MG, IC, RB, and MB were less than 1, thus indicating that their adsorptions were favorable [55].

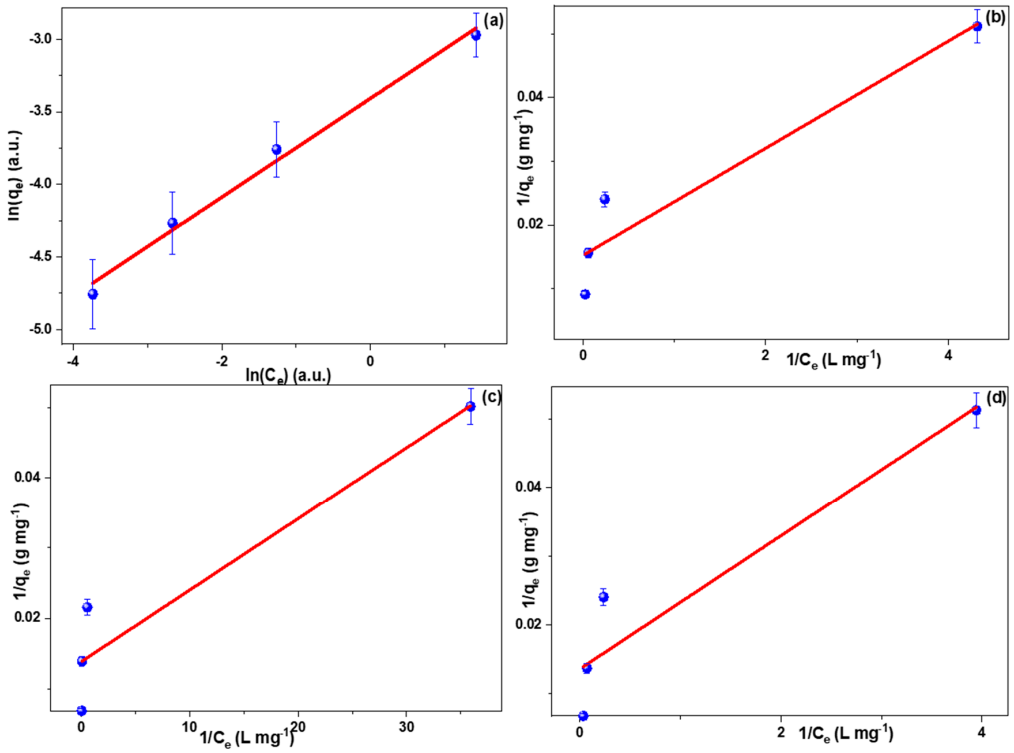

Figure 6. The LIM investigations for the adsorption of (**a**) MG, (**b**) IC, (**c**) RB, and (**d**) MB on the TPCNPs using 10, 25, 50, and 100 mg L^{-1} dye solutions at 298, 308, and 318 °K.

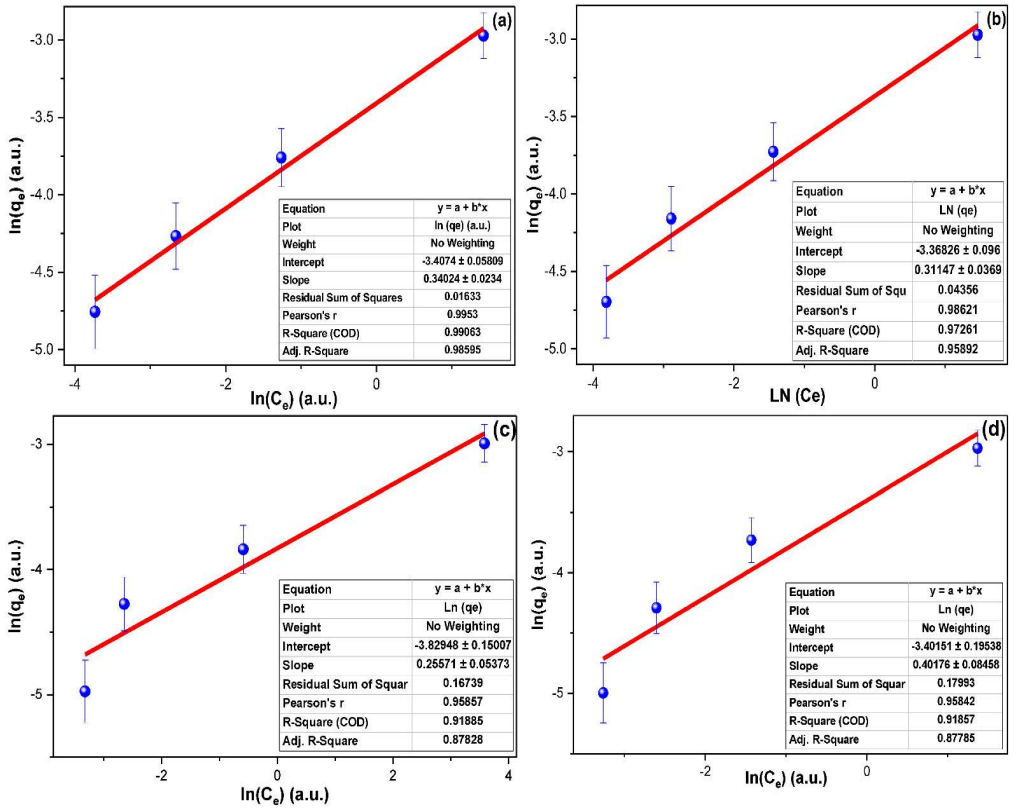

Figure 7. The FIM investigations for the adsorption of (**a**) MG, (**b**) IC, (**c**) RB, and (**d**) MB on the TPCNPs at 25 °C.

Table 3. The Isotherms and thermodynamic parameters for the adsorption of MG, IC, RB, and MB adsorption on the prepared TPCNPs.

Adsorption Isotherms						
Isotherm Model →		Langmuir			Freundlich	
Dye ↓	R^2 (a.u.)	K_L (L mg^{-1})	q_m (mg g^{-1})	R^2(a.u.)	K_f (L mg^{-1})	n^{-1} (a.u.)
MG	0.928	71.276	1.542	0.991	0.033	0.340
IC	0.916	65.445	1.821	0.973	0.034	0.311
RB	0.908	72.098	13.733	0.919	0.022	0.256
MB	0.897	73.801	1.400	0.919	0.033	0.402
Thermodynamic Parameters						
			MG			
Fed conc. (mg L^{-1})	ΔH° (Kj mol^{-1})	ΔS° (kJ mol^{-1})	ΔG° (kJ mol^{-1}) 298 K	ΔG° (kJ mol^{-1}) 308 K	ΔG° (kJ mol^{-1}) 318 K	R^2
10	−103.125	−0.314	−9.453	−6.309	−3.166	0.975
25	−30.022	−0.086	−4.351	−3.490	−2.628	0.954
50	−42.628	−0.135	−2.424	−1.075	0.274	0.953
100	−34.139	−0.112	−0.906	0.209	1.324	0.975
			IC			
10	−148.286	−0.466	−9.547	−4.892	−0.236	0.989
25	−76.294	−0.244	−3.688	−1.251	1.185	0.964
50	−26.268	−0.049	−11.556	−11.062	−10.568	0.961
100	−46.201	−0.153	−0.606	0.924	2.454	0.974
			RB			
10	−182.242	−0.564	−14.138	−8.497	−2.856	0.970
25	−67.406	−0.210	−4.915	−2.818	−0.721	0.955
50	−46.729	−0.156	−0.368	1.188	2.744	0.995
100	−64.772	−0.216	−0.503	1.654	3.811	0.999
			MB			
10	−71.474	−0.211	−8.646	−6.538	−4.430	0.999
25	−64.006	−0.203	−3.596	−1.568	0.459	0.999
50	−54.862	−0.178	−1.709	0.075	1.859	0.999
100	−56.198	−0.185	−0.997	0.855	2.707	0.990

2.5. Adsorption Thermodynamics

The thermodynamics of MG, IC, RB, and MB adsorptions on TPCNPs were examined. The entropy (Δ$S°$) and enthalpy (Δ$H°$) of sorptions were computed from the plot of Equation (11) (Figure 8). A 0.0081345 kJ mol^{-1} was utilized in all calculations as a gas-constant value (R), and the makeup of Δ$H°$, and Δ$S°$ values into Equation (12) produced the Gibbs free energy (Δ$G°$) (Table 3).

$$\ln K_c = \frac{\Delta H^{\,o}}{RT} + \frac{\Delta S^{\,o}}{R} \quad (11)$$

$$\Delta G^{\,o} = \Delta H^{\,o} - T\,\Delta S^{\,o} \quad (12)$$

The negative Δ$H°$ values for MG, IC, RB, and MB adsorption indicated the sorption's exothermic nature for all sorbent–sorbate systems. Moreover, the negative Δ$G°$ at 298 °K showed the spontaneity of sorptions at low temperatures, which is another support for the exothermic nature finding. In addition, the average Δ$H°$ values of less than 80 kJ mol^{-1} for MG, IC, RB, and MB indicated that the sorption was physical [56–60].

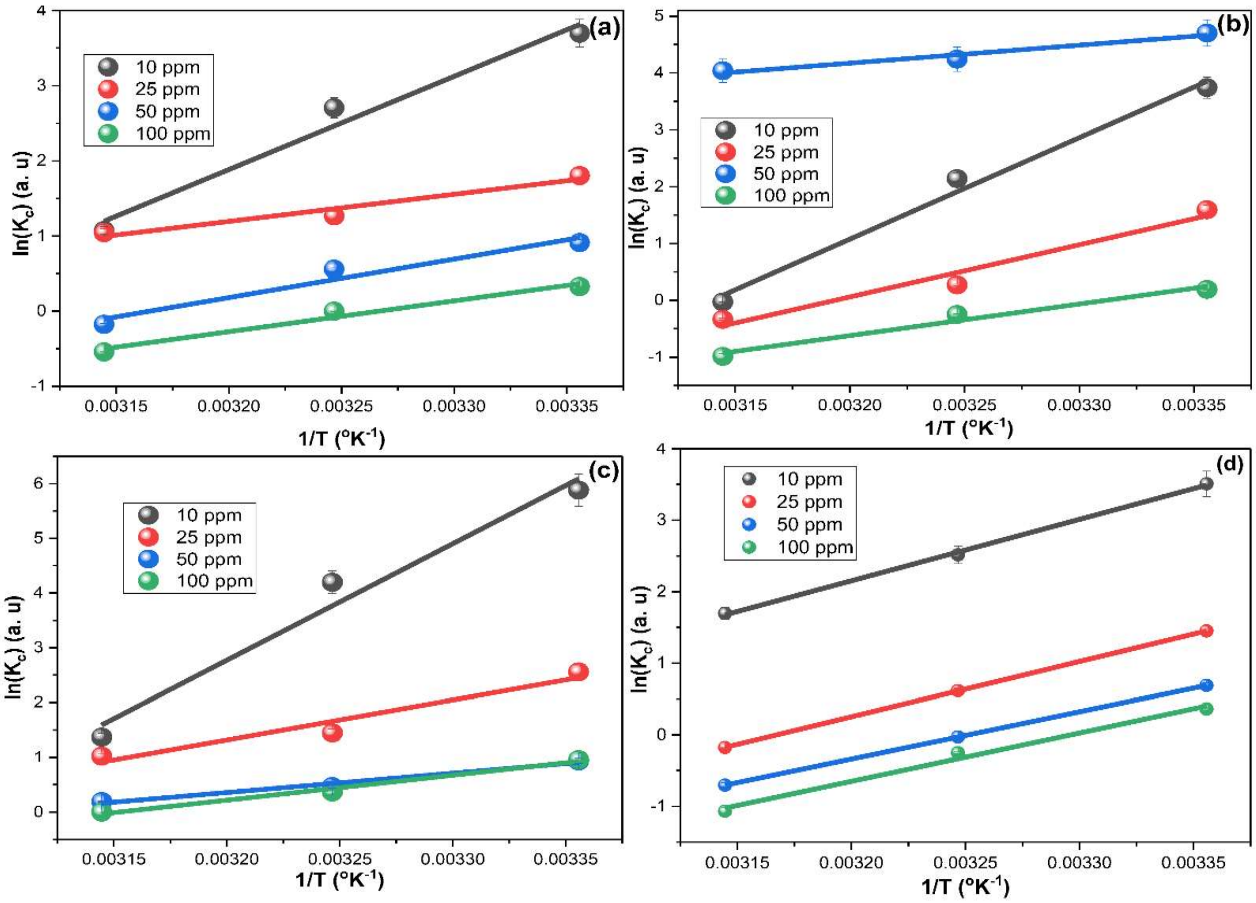

Figure 8. Thermodynamic investigations for the adsorption of (**a**) MG, (**b**) IC, (**c**) RB, and (**d**) MB on the TPCNPs at 298, 308, and 318 °K by employing 10, 25, 50, and 100 mg L^{-1} solutions form each dye.

2.6. Application to Natural Water Samples and Regeneration of TPCNPs

The GW had a total dissolved solids (TDS) value of 1.05 g L^{-1}, a temperature of 24.5 °C, and a pH value of 7.23. On the other hand, the SW showed a TDS value of 33.84 g L^{-1}, a temperature of 27.4 °C, and a pH value of 7.46. Figure 9a shows the removal of MG, IC, RB, and MB from contaminated GW and SW samples. The TPCNPs showed an average removal efficiency of 99.3% and 98.8% for the four dyes from 5 mg L^{-1} polluted SW and GW, and 97.2 and 95.8 from the 10 mg L^{-1} concentration. As the sorption of MG, IC, RB, and MB adsorption on the prepared TPCNPs fitted the LFDM, the high saline concentration of SW may suppress the dyes' diffusions and cause a decrease in removal efficiency from the SW compared to the GW. Since organic pollutants are unacceptable at any concentration, the same SW and GW samples were retreated with half the amount of virgin TPCNPs. Complete remediation was attained for all contaminated water samples.

Furthermore, the regeneration-reusability investigation was carried out for the TPCNPs. As the TPCNPs showed lower adsorption capacity in the alkaline media, the used sorbent was filtered and sonicated for 10 min with 10 mL of 1M sodium hydroxide. Then, the TPCNPs were sonicated with 10 mL ethanol, filtered, rinsed with distilled water, dried at 110 °C for 1.0 h, and used for the next round. In order to eliminate the effect of TPCNP loss during the regeneration investigation, the volumes of solutions were reduced proportionally to conserve the sorbent: solution ratio. The removal efficiency of the virgin TPCNPs was used as 100%, and the efficiencies and the subsequent rounds were calculated accordingly (Figure 9b) [61]. The average efficiency of TPCNPs within the five cycles was 91.78, 94.18, 93.76, and 94.35% for MG, IC, RB, and MB, respectively. The relative standard deviation (RSD) for the five rounds of removing MG, IC, RB, and MB was 6.40, 4.25, 5.70, and 5.48%, respectively. Figure 9c,d illustrates the surficial characteristics of the

regenerated TPCRNPs via SEM images. The obtained particle size range of 52.0 to 82.0 nm indicated a slight particle size change that may be caused via agglomeration of TPCNPs in the aqueous medium. The agreement of all sorbent–sorbate systems to the LFDM shows that the pollutants easily penetrate to the inner shells with high affinity to the TPCNP. These factors may hinder the recovery process and cause efficiency to decrease in the last reuse cycles [51,62].

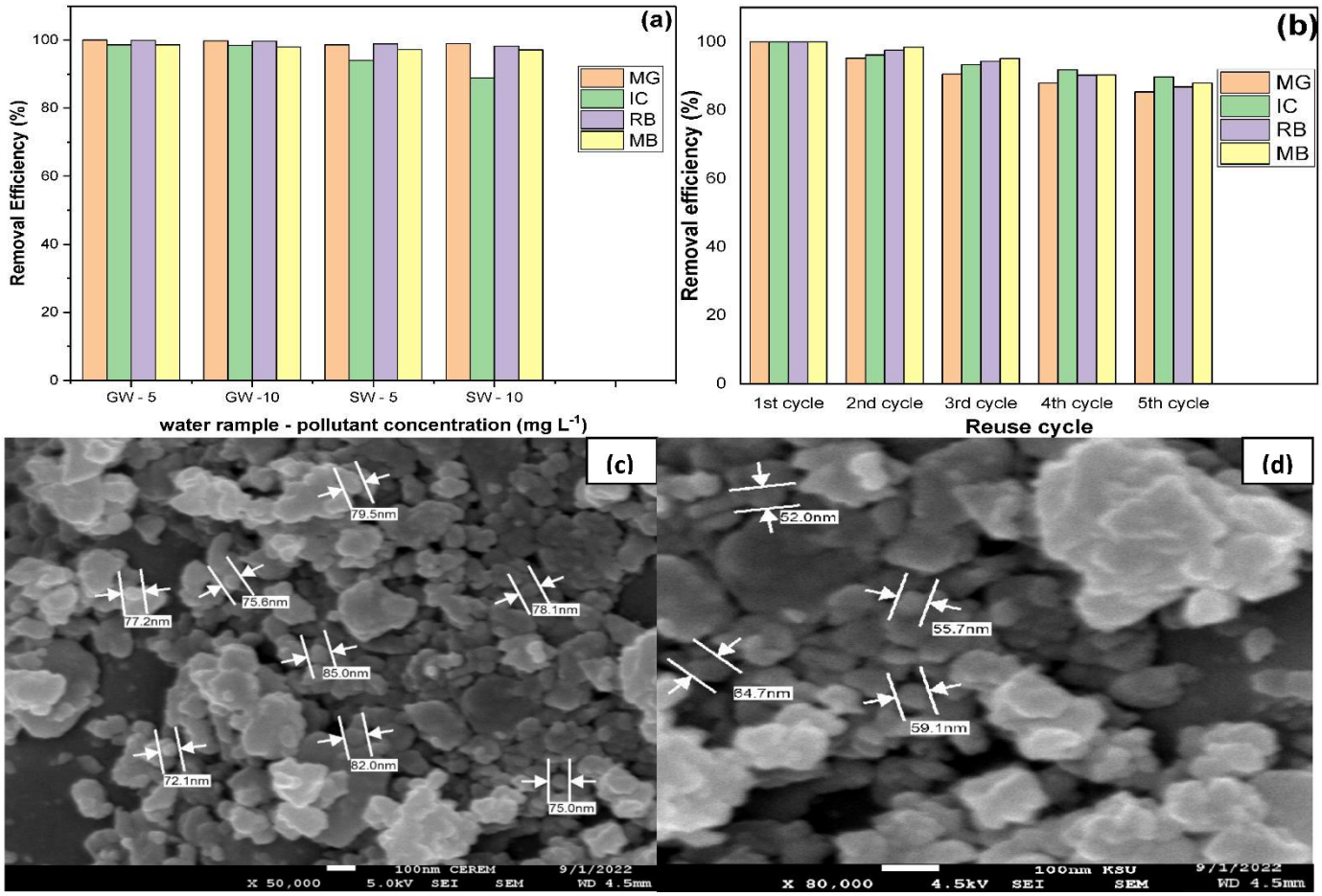

Figure 9. (**a**) The removal of MG, IC, RB, and MB from the groundwater (GW) and seawater samples artificially contaminated by 5 and 10 mg L^{-1} dye concentrations; (**b**) the regeneration-reusability study for the TPCNPs in removing MG, IC, RB, and MB; (**c**,**d**) SEM images for the regenerated TPCNPs.

3. Materials and Methods

3.1. Materials

Nitric acid 69% was provided from LOBA-CHEM, Mumbai, India. Waste toilet paper (TP) was gathered from a bathroom basket at Riyadh-KSA. The IC and RB were from Merck, Germany, while the MG and MB were from LOBA-CHEM, Mumbai, India.

3.2. Preparation of Carbon Nanoparticles

About 50.0 g of TPW was calcined in a tubular furnace at 900 °C under a nitrogen stream (50.0 mL/h). The resulting TP-CRM was boiled in 250 mL of 5.0 M nitric acid for 2.0 h. The product was filtered, washed with distilled water (to pH ≈ 6.5), and dried at 110 °C for 3.0 h. Five stainless steel balls (1.0 cm in diameter) were transferred to a 50 mL stainless steel crucible, then 10.0 gm of the TP-AcC was added. The ball-milling machine was operated at 500 rounds per minute for 10 h, and the toilet paper's carbon nanoparticles (TPCNPs) were collected for further work.

3.3. Characterization of Carbon Nanoparticles

The TPCNPs were analyzed utilizing scanning electron energy dispersive X-ray spectroscopy (SEM-EDS, JSM-IT300), an X-ray diffractometer (Bruker, D8 Advance; Billerica, MA, USA), an FTIR spectrophotometer (Bruker TENSOR—Germany), and a surface analyzer (Micromeritics analyzer ASAP 2020).

3.4. Adsorption Investigation

The TPCNPs have been studied as adsorbents for removing IC, RB, MG, and MB from water. A 50 mg L^{-1} solution was selected at a relatively high concentration to examine the sorbent capacity. A total of 50 mg of TPCNP was stirred (700 rpm) with 120 mL of 50 mg L^{-1} dye solution to investigate the contact time influence on the sorption process at 25 °C. A UV-Vis-spectrophotometer (Shimadzu-2600i) was employed to determine the pollutant concentrations. Moreover, the impact of initial concentration on the sorption trends was studied using 10, 25, 50, and 100 mg L^{-1} solutions in order to test the TPCNPs' efficiency at a wide concentration range. Furthermore, the previously mentioned concentrations were utilized to examine the influence of the temperature on sorption at 20, 35, and 50 °C, which were selected to obtain a clear difference in the temperature effect. Moreover, the pH effect on the dye sorption was inspected within the pH range of 2.0 to 10.0. The adsorption percentage of pollutants (*Ads*%) and the adsorption capacity (q_t) were computed by Equations (13) and (14).

$$Ads\% = \frac{(C_o - C_t)}{C_o} \times 100 \quad (13)$$

$$q_t = \frac{(C_o - C_t)\ V}{M} \quad (14)$$

C_o (mg L^{-1}): initial dye concentration; C_t (mg L^{-1}): remained dye concentration; V (L): solution's volume; M (g): sorbent's mass.

3.5. Application to Natural Water Samples

Seawater and groundwater samples (SW and GW) were collected from the Arabic Gulf, Dammam Coast, KSA, and Al Majma'ah city (185 km north of Riyadh, KSA). SW and GW were spiked with an appropriate volume of concentrated dye solution to prepare 5.0 and 10.0 mg L^{-1} of each dye separately. The effect of the SW and GW matrix on determining sample concentrations was eliminated by using each prepared solution as a standard for its sample, and thereafter the pollutant concentration was computed via the comparative method.

4. Conclusions

As a low-cost precursor, toilet paper waste was used to fabricate carbon nanoparticle TPCNPs via carbonization ball milling processes. The prepared TPCNPs' size was less than 100 nm and possessed a surface area of 264.52 $m^2\ g^{-1}$. The batch methodology was utilized to study the removal of MG, IC, RB, and MB from water. The adsorption of MG and IC fitted the PSFO kinetic model, while RB and MB fitted PSSO; all sorbent–sorbate systems in this study followed the LFDM with good agreement. MG, IC, RB, and MB adsorptions on the TPCNPs showed better agreement with the FIM. According to the thermodynamic investigations, the four dyes' removals were exothermic, spontaneous, and physisorption. The TPCNPs removed MG, IC, RB, and MB from the spiked SW and GW, and a double treatment resulted in the complete remediation of contaminated water. The reusability study revealed excellent performance consistency during five consecutive uses. Therefore, prepared TPCNPs are recommended for treating industrial and polluted water resources as a low-cost sorbent.

Author Contributions: Conceptualization and data curation by B.Y.A.; methodology, validation, formal analysis, investigation, original draft preparation, review, B.Y.A. and M.R.E.; editing, visualization supervision, funding acquisition, B.Y.A. All authors have read and agreed to the published version of the manuscript.

Funding: This research was funded by the Deanship of Scientific Research, Imam Mohammad Ibn Saud Islamic University, Saudi Arabia, Grant No. (20-13-12-019).

Institutional Review Board Statement: Not applicable.

Conflicts of Interest: The authors declare no conflict of interest.

References

1. Rahbar-Shamskar, K.; Azar, P.A.; Rashidi, A.; Baniyaghoob, S.; Yousefi, M. Synthesis of micro/mesoporous carbon adsorbents by in-situ fast pyrolysis of reed for recovering gasoline vapor. *J. Clean. Prod.* **2020**, *259*, 120832. [CrossRef]
2. Silva, A.R.; Cavaleiro, A.J.; Soares, O.S.G.; Braga, C.S.; Salvador, A.F.; Pereira, M.F.R.; Alves, M.M.; Pereira, L. Detoxification of ciprofloxacin in an anaerobic bioprocess supplemented with magnetic carbon nanotubes: Contribution of adsorption and biodegradation mechanisms. *Int. J. Mol. Sci.* **2021**, *22*, 2932. [CrossRef]
3. Bożęcka, A.; Orlof-Naturalna, M.; Kopeć, M. Methods of Dyes Removal from Aqueous Environment. *J. Ecol. Eng.* **2021**, *22*, 111–118. [CrossRef]
4. Ho, S.; Protection, E. Removal of Dyes from Wastewater by Adsorption onto Activated Carbon: Mini Review. *J. Geosci. Environ. Prot.* **2020**, *8*, 120. [CrossRef]
5. Sivaprakasha, S.; Kumarb, P.S.; Krishnac, S. Adsorption study of various dyes on Activated Carbon Fe_3O_4 Magnetic Nano Composite. *Int. J. Appl. Chem.* **2017**, *13*, 255–266.
6. Topare, N.S.; Bokil, S.A. Adsorption of textile industry effluent in a fixed bed column using activated carbon prepared from agro-waste materials. *Mater. Today Proc.* **2021**, *43*, 530–534. [CrossRef]
7. Yurtsever, A.; Basaran, E.; Ucar, D.; Sahinkaya, E. Self-forming dynamic membrane bioreactor for textile industry wastewater treatment. *Sci. Total Environ.* **2021**, *751*, 141572. [CrossRef] [PubMed]
8. Feng, Q.; Gao, B.; Yue, Q.; Guo, K. Flocculation performance of papermaking sludge-based flocculants in different dye wastewater treatment: Comparison with commercial lignin and coagulants. *Chemosphere* **2021**, *262*, 128416. [CrossRef] [PubMed]
9. Othman, M.H.D.; Adam, M.R.; Kamaludin, R.; Ismail, N.J.; Rahman, M.A.; Jaafar, J. Advanced Membrane Technology for Textile Wastewater Treatment. In *Membrane Technology Enhancement for Environmental Protection and Sustainable Industrial Growth*; Springer: Berlin/Heidelberg, Germany, 2021; pp. 91–108.
10. Chowdhury, M.F.; Khandaker, S.; Sarker, F.; Islam, A.; Rahman, M.T.; Awual, M.R. Current treatment technologies and mechanisms for removal of indigo carmine dyes from wastewater: A review. *J. Mol. Liq.* **2020**, *318*, 114061. [CrossRef]
11. Harrache, Z.; Abbas, M.; Aksil, T.; Trari, M. Thermodynamic and kinetics studies on adsorption of Indigo Carmine from aqueous solution by activated carbon. *Microchem. J.* **2019**, *144*, 180–189. [CrossRef]
12. Oberoi, A.S.; Jia, Y.; Zhang, H.; Khanal, S.K.; Lu, H. Insights into the fate and removal of antibiotics in engineered biological treatment systems: A critical review. *Environ. Sci. Technol.* **2019**, *53*, 7234–7264. [CrossRef]
13. Jones, O.A.; Lester, J.N.; Voulvoulis, N. Pharmaceuticals: A threat to drinking water? *Trends Biotechnol.* **2005**, *23*, 163–167. [CrossRef] [PubMed]
14. Hussin, F.; Aroua, M.K.; Kassim, M.A.; Ali, U.F. Transforming Plastic Waste into Porous Carbon for Capturing Carbon Dioxide: A Review. *Energies* **2021**, *14*, 8421. [CrossRef]
15. Rasheed, T.; Ahmad, N.; Ali, J.; Hassan, A.A.; Sher, F.; Rizwan, K.; Iqbal, H.M.N.; Bilal, M. Nano and micro architectured cues as smart materials to mitigate recalcitrant pharmaceutical pollutants from wastewater. *Chemosphere* **2021**, *274*, 129785. [CrossRef]
16. Sabzehmeidani, M.M.; Mahnaee, S.; Ghaedi, M.; Heidari, H.; Roy, V.A.L. Carbon based materials: A review of adsorbents for inorganic and organic compounds. *Mater. Adv.* **2021**, *2*, 598–627. [CrossRef]
17. Jjagwe, J.; Olupot, P.W.; Menya, E.; Kalibbala, H.M. Synthesis and application of Granular activated carbon from biomass waste materials for water treatment: A review. *J. Bioresour. Bioprod.* **2021**, *6*, 292–322. [CrossRef]
18. Foroutan, R.; Peighambardoust, S.J.; Peighambardoust, S.H.; Pateiro, M.; Lorenzo, J.M. Adsorption of Crystal Violet Dye Using Activated Carbon of Lemon Wood and Activated Carbon/Fe_3O_4 Magnetic Nanocomposite from Aqueous Solutions: A Kinetic, Equilibrium and Thermodynamic Study. *Molecules* **2021**, *26*, 2241. [CrossRef]
19. Kafil, M.; Nasab, B.; Moazed, H.; Jokiniemi, J.; Laehde, A.; Bhatnagar, A. Efficient removal of azo dyes from water with chitosan/carbon nanoflower as a novel nanocomposite synthesized by pyrolysis technique. *Desalin. Water Treat.* **2019**, *142*, 308–320. [CrossRef]
20. Wan, S.; Bi, H.; Sun, L. Graphene and carbon-based nanomaterials as highly efficient adsorbents for oils and organic solvents. *Nanotechnol. Rev.* **2016**, *5*, 3–22. [CrossRef]
21. Tavakkoli, M.; Flahaut, E.; Peljo, P.; Sainio, J.; Davodi, F.; Lobiak, E.V.; Mustonen, K.; Kauppinen, E.I. Mesoporous single-atom-doped graphene–carbon nanotube hybrid: Synthesis and tunable electrocatalytic activity for oxygen evolution and reduction reactions. *ACS Catal.* **2020**, *10*, 4647–4658. [CrossRef]
22. Xu, W.; Dong, X.; Wang, Y.; Zheng, N.; Zheng, B.; Lin, Q.; Zhao, Y. Controllable Synthesis of MoS_2/Carbon Nanotube Hybrids with Enlarged Interlayer Spacings for Efficient Electrocatalytic Hydrogen Evolution. *ChemistrySelect* **2020**, *5*, 13603–13608. [CrossRef]
23. Fu, S.; Chen, X.; Liu, P. Preparation of CNTs/Cu composites with good electrical conductivity and excellent mechanical properties. *Mater. Sci. Eng. A* **2019**, *771*, 138656. [CrossRef]

24. Verma, B.; Goel, S.; Balomajumder, C. Multiwalled CNTs for Cr (VI) removal from industrial wastewater: An advanced study on adsorption, kinetics, thermodynamics for the comparison between the embedded and non-embedded carboxyl group. *Can. J. Chem. Eng.* **2021**, *99*, 281–293. [CrossRef]
25. Elamin, M.R.; Abdulkhair, B.Y.; Elzupir, A.O. Insight to aspirin sorption behavior on carbon nanotubes from aqueous solution: Thermodynamics, kinetics, influence of functionalization and solution parameters. *Sci. Rep.* **2019**, *9*, 1–10.
26. Supriya, S.; Sriram, G.; Ngaini, Z.; Kavitha, C.; Kurkuri, M.; De Padova, I.P.; Hegde, G. The role of temperature on physical–chemical properties of green synthesized porous carbon nanoparticles. *Waste Biomass Valorization* **2019**, *11*, 3821–3831. [CrossRef]
27. Ibrahimov, H.; Amirov, F.; Huseynov, H.; Ibragimova, Z.; Zamanova, L.; Asadzadeh, R.; Jabarov, S.H. Carbon nanotubes obtained from natural gas by CVD. *J. Surf. Investig. X-ray Synchrotron Neutron Tech.* **2019**, *13*, 1244–1247. [CrossRef]
28. Almufarij, R.S.; Abdulkhair, B.Y.; Salih, M.; Aldosari, H.; Aldayel, N.W. Optimization, Nature, and Mechanism Investigations for the Adsorption of Ciprofloxacin and Malachite Green onto Carbon Nanoparticles Derived from Low-Cost Precursor via a Green Route. *Molecules* **2022**, *27*, 4577. [CrossRef] [PubMed]
29. Breland, O.P.J.S. *A Laboratory Manual Of Comparative Anatomy/ Barker, Kenneth & Breland, Osmond*; Mcgraw-Hill Book Inc.: New York, NY, USA, 1980.
30. Mote, V.; Purushotham, Y.; Dole, B.N. Williamson-Hall analysis in estimation of lattice strain in nanometer-sized ZnO particles. *J. Theor. Appl. Phys.* **2012**, *6*, 1–8. [CrossRef]
31. Ilyas, S.; Abdullah, B.; Tahir, D. X-ray diffraction analysis of nanocomposite Fe_3O_4/activated carbon by Williamson–Hall and size-strain plot methods. *Nano-Struct. Nano-Objects* **2019**, *20*, 100396. [CrossRef]
32. Silverstein, R.M.; Bassler, G.C. *Spectrometric Identification of Organic Compounds*; State University New York: Albany, NY, USA, 2021.
33. Pavia, D.L.; Lampman, G.M.; Kriz, G.S.; Vyvyan, J.A. *Introduction to Spectroscopy*; Cengage Learning Acquisitions, Inc.: Boston, MA, USA, 2014.
34. Thommes, M.; Kaneko, K.; Neimark, A.V.; Olivier, J.P.; Rodriguez-Reinoso, F.; Rouquerol, J.; Sing, K.S. Physisorption of gases, with special reference to the evaluation of surface area and pore size distribution (IUPAC Technical Report). *Pure Appl. Chem.* **2015**, *87*, 1051–1069. [CrossRef]
35. Wang, S.-C. Fine Activated Carbon from Rubber Fruit Shell Prepared by Using $ZnCl_2$ and KOH Activation. *Appl. Sci.* **2021**, *11*, 3994.
36. Bandura, L.; Panek, R.; Madej, J.; Franus, W. Synthesis of zeolite-carbon composites using high-carbon fly ash and their adsorption abilities towards petroleum substances. *Fuel* **2020**, *283*, 119173. [CrossRef]
37. Yang, J.; Wang, X.; Dai, W.; Lian, X.; Cui, X.; Zhang, W.; Zhang, K.; Lin, M.; Zou, R.; Loh, K.; et al. From micropores to ultra-micropores inside hard carbon: Toward enhanced capacity in room-/low-temperature sodium-ion storage. *Nano-Micro Lett.* **2021**, *13*, 1–14. [CrossRef] [PubMed]
38. Zhang, J.-Z.; Huang, X.-L. Effect of temperature and salinity on phosphate sorption on marine sediments. *Environ. Sci. Technol.* **2011**, *45*, 6831–6837. [CrossRef] [PubMed]
39. Flower, H.; Rains, M.; Lewis, D.; Zhang, J.-Z.; Price, R. Saltwater intrusion as potential driver of phosphorus release from limestone bedrock in a coastal aquifer. *Environ. Sci. Technol.* **2017**, *184*, 166–176. [CrossRef]
40. Elamin, M.R.; Abdulkhair, B.Y.; Elzupir, A.O. Removal of ciprofloxacin and indigo carmine from water by carbon nanotubes fabricated from a low-cost precursor: Solution parameters and recyclability. *Ain Shams Eng. J.* **2022**, 101844. [CrossRef]
41. Igwegbe, C.A.; Oba, S.N.; Aniagor, C.O.; Adeniyi, A.G.; Ighalo, J.O. Adsorption of ciprofloxacin from water: A comprehensive review. *J. Ind. Eng. Chem.* **2020**, *93*, 57–77. [CrossRef]
42. de Oliveira Brito, S.M.; Andrade, H.M.C.; Soares, L.F.; de Azevedo, R.P. Brazil nut shells as a new biosorbent to remove methylene blue and indigo carmine from aqueous solutions. *J. Hazard. Mater.* **2010**, *174*, 84–92. [CrossRef] [PubMed]
43. Lakshmi, U.R.; Srivastava, V.C.; Mall, I.D.; Lataye, D.H. Rice husk ash as an effective adsorbent: Evaluation of adsorptive characteristics for Indigo Carmine dye. *J. Environ. Manag.* **2009**, *90*, 710–720. [CrossRef]
44. Mittal, A.; Mittal, J.; Kurup, L. Batch and bulk removal of hazardous dye, indigo carmine from wastewater through adsorption. *J. Hazard. Mater.* **2006**, *137*, 591–602. [CrossRef]
45. Prado, A.G.; Torres, J.D.; Faria, E.A.; Dias, S.C. Comparative adsorption studies of indigo carmine dye on chitin and chitosan. *J. Colloid Interface Sci.* **2004**, *277*, 43–47. [CrossRef]
46. Jawad, A.H.; Abdulhameed, A.S.; Wilson, L.D.; Syed-Hassan, S.S.A.; ALOthman, Z.A.; Khan, M.R. High surface area and mesoporous activated carbon from KOH-activated Dragon fruit peels for methylene blue dye adsorption: Optimization and mechanism study. *Chin. J. Chem. Eng.* **2021**, *32*, 281–290. [CrossRef]
47. Ahmed, R.; Hossain, M.A. Optimization of a fixed bed column adsorption of Fast Green dye on used black tea leaves from aqueous solution. *J. Iran. Chem. Soc.* **2022**, *19*, 381–391. [CrossRef]
48. Renita, A.A.; Amarnath, D.J.; Duraikannu, S.L. Synthesis of peanut-shell magnetized biocarbon for acid fuchsin dye removal. *Mater. Today Proc.* **2021**, *43*, 3075–3078. [CrossRef]
49. Naghizadeh, A.; Karimi, A.; Derakhshani, E.; Esform, A. Single-walled carbon nanotubes (SWCNTs) as an efficient adsorbent for removal of reactive dyes from water solution: Equilibrium, kinetic, and thermodynamic. *Environ. Qual. Manag.* **2021**, *31*, 133–140. [CrossRef]
50. Ofomaja, A.E.; Naidoo, E.B.; Pholosi, A. Intraparticle diffusion of Cr (VI) through biomass and magnetite coated biomass: A comparative kinetic and diffusion study. *S. Afr. J. Chem. Eng.* **2020**, *32*, 39–55.

51. An, B. Cu (II) and As (V) adsorption kinetic characteristic of the multifunctional amino groups in chitosan. *Processes* **2020**, *8*, 1194. [CrossRef]
52. Magdy, Y.; Altaher, H. Kinetic analysis of the adsorption of dyes from high strength wastewater on cement kiln dust. *J. Environ. Chem. Eng.* **2018**, *6*, 834–841. [CrossRef]
53. Konggidinata, M.I.; Chao, B.; Lian, Q.; Subramaniam, R.; Zappi, M.; Gang, D.D. Equilibrium, kinetic and thermodynamic studies for adsorption of BTEX onto Ordered Mesoporous Carbon (OMC). *J. Hazard. Mater.* **2017**, *336*, 249–259. [CrossRef]
54. Khayyun, T.S.; Mseer, A.H. Comparison of the experimental results with the Langmuir and Freundlich models for copper removal on limestone adsorbent. *Appl. Water Sci.* **2019**, *9*, 1–8. [CrossRef]
55. Acharya, J.; Sahu, J.; Mohanty, C.; Meikap, B. Removal of lead (II) from wastewater by activated carbon developed from Tamarind wood by zinc chloride activation. *Chem. Eng. J.* **2009**, *149*, 249–262. [CrossRef]
56. Letshwenyo, M.W.; Mokgosi, S. Investigation of water treatment sludge from drinking water treated with Zetafloc 553I coagulant for phosphorus removal from wastewater. *J. Environ. Manag.* **2021**, *282*, 111909. [CrossRef] [PubMed]
57. Demirbas, O.; Calimli, M.H.; Kuyuldar, E.; Alma, M.H.; Nas, M.S.; Sen, F. Equilibrium, kinetics, and thermodynamic of adsorption of enzymes on diatomite clay materials. *BioNanoScience* **2019**, *9*, 474–482. [CrossRef]
58. Aarab, N.; Hsini, A.; Essekri, A.; Laabd, M.; Lakhmiri, R.; Albourine, A. Removal of an emerging pharmaceutical pollutant (metronidazole) using PPY-PANi copolymer: Kinetics, equilibrium and DFT identification of adsorption mechanism. *Groundw. Sustain. Dev.* **2020**, *11*, 100416. [CrossRef]
59. Vasudevan, S.; Lakshmi, J. Studies relating to an electrochemically assisted coagulation for the removal of chromium from water using zinc anode. *Water Supply* **2011**, *11*, 142–150. [CrossRef]
60. Inglezakis, V.J.; Zorpas, A.A. Heat of adsorption, adsorption energy and activation energy in adsorption and ion exchange systems. *Desalin. Water Treat.* **2012**, *39*, 149–157. [CrossRef]
61. Wang, N.; Han, Y.; Li, S. Adsorption characteristic of Cr (VI) onto different activated coal fly ashes: Kinetics, thermodynamic, application feasibility, and error analysis. *Water Air Soil Pollut.* **2019**, *230*, 1–13. [CrossRef]
62. Hameed, B.; El-Khaiary, M. Malachite green adsorption by rattan sawdust: Isotherm, kinetic and mechanism modeling. *J. Hazard. Mater.* **2008**, *159*, 574–579. [CrossRef]